Adhesion and Friction of Polymer Surfaces: The Effect of Chain Ends

Nianhuan Chen, Nobuo Maeda,† Matthew Tirrell, and Jacob Israelachvili*

Departments of Chemical Engineering and Materials, and the Materials Research Laboratory, College of Engineering, University of California, Santa Barbara, California 93106

Received November 3, 2004; Revised Manuscript Received January 4, 2005

ABSTRACT: Using a surface forces apparatus we studied the adhesion and friction of glassy polystyrene (PS) and poly(vinylbenzyl chloride) (PVBC) surfaces having various molecular weights (MW) from 2 000 000 to 1240 Da. Cross-linking of high MW polymers leads to lower adhesion and friction relative to the untreated polymers, whereas scission (bond-breaking) leads to higher adhesion and friction. "Asymmetric" bond-broken against cross-linked surfaces behave intermediately between the two "symmetric" systems. Both the friction and adhesion of untreated polymers increase with decreasing MW, often resulting in irreversible damage during sliding or separation. We conclude that the population of the chain "ends" at the surfaces is the most important factor that determines the adhesion, adhesion hysteresis, friction, and wear between two polymer surfaces. Segment polarity and layer thickness play secondary roles.

Introduction

The surface energy γ of a solid is one of the most important and fundamental parameter that characterizes its surface, and much effort has gone into measurement of the surface energies of different solids. The various techniques used include the cleaving of single crystals in ultrahigh vacuum (UHV), "Zisman plots" with a number of liquids that have different contact angles on the solid,[1−4] and contact mechanics equations such as "JKR plots" where the contact area vs load and the adhesion or pull-off force are measured between a sphere and a flat surface.[5−12] Regardless of which method is used, there is almost always some energy dissipation where the measured adhesion energy or force between two solid surfaces, for example, is higher—sometimes by orders of magnitude—than the thermodynamic value. In contact angle measurements involving liquids, dissipation manifests itself as contact angle hysteresis, which is related to adhesion energy hysteresis seen with solids. Contact angle and adhesion hysteresis can also be due to topographical and chemical heterogeneities at surfaces. However, even with perfectly homogeneous and smooth surfaces, energy dissipation, leading to hysteresis effects, can result from *nonequilibrium* (time and rate dependent) structural rearrangements of molecules at or near a surface or interface, as well as viscoelastic effects associated with the bulk deformations of adhering surfaces. Both of these mechanisms also occur when two solid bodies slide against each other, i.e., during frictional sliding, regardless of whether the two surfaces adhere or not.[13] For adhering surfaces, the friction force can be thought of as arising from the continuous "cycles" of forming and breaking of bonds, where the breaking costs more energy than the making; i.e., the processes are inherently hysteretic or "the cycle is irreversible".

There has been a steady accumulation of data in the field of adhesion and friction that suggests that these complex and traditionally macroscopic phenomena could be understood from the behavior of the molecules or even submolecular groups at the adhering or sliding interfaces.[14−16] For glassy polymer systems, we previously reported that both the adhesion and friction forces between two PS or PVBC surfaces are least when the surfaces are cross-linked and the largest for surfaces that have been cross-linked then subjected to chain scission or "bond breaking".[12] It was suggested that interpenetration of polymer chain ends or loops across the contacting or shearing interfaces is likely to be responsible for the unexpectedly large effects observed, but a systematic study covering a larger range of molecular weights—which would be needed to fully characterize these effects and distinguish between the contributions of ends and loops—was not done. This is the main purpose of this work.

It is generally expected that increased polarity leads to increased adhesion, adhesion hysteresis and friction.[7,17] A further important issue of this work concerns the UV treatment of polymers such as PS to induce chain scission, but which also results in oxidization of the surfaces.[18,19] Since the increased polarity of the surface groups is expected to affect the adhesion and friction forces, and it was considered important to also distinguish between this contribution and that due to the increased density of chain ends.

To test the relative importance of chain ends vs loops without the complication arising from UV treatment, we systematically studied the adhesion and friction of a series of untreated (not cross-linked and not bond-broken) low molecular weight PS surfaces. The lower the MW, the higher the fraction of the chain ends at the surfaces.[28] Thus, if the number of chain ends at the surfaces is the most important factor, we should expect a gradual *increase* of the adhesion hysteresis and friction forces as the MW is reduced (unless the molecular weight is so low that the PS is no longer glassy, becomes liquidlike, resulting in a dramatic *decrease* in these forces). In all, our experiments covered PS molecular weights that ranged over more than 3 orders of magnitude.

Materials and Methods

Preparation of Polymer Surfaces. Polystyrene (PS) and poly(vinylbenzyl chloride) (PVBC) were purchased from Sigma-

* To whom correspondence should be addressed at the Department of Chemical Engineering, College of Engineering, University of California, Santa Barbara. E-mail: jacob@engineering.ucsb.edu. Fax: 805-893-7870. Telephone: 805-893-8407.

† Present address: Department of Applied Mathematics, Research School of Physical Sciences and Engineering, Australian National University, Canberra, ACT0200, Australia.

10.1021/ma047733e CCC: $30.25
Published on Web 03/25/2005

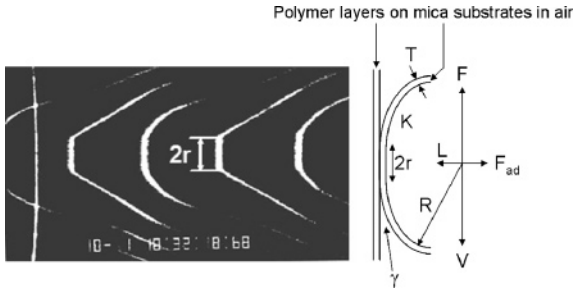

Figure 1. Typical FECO fringes of polymer surfaces in the adhesive contact (left) and the schematic picture that defines different parameters in the system (right); the contact radius r (about 30 μm in this figure), elastic modulus K, the interfacial energy γ, the radius of the curvature of the surface R, and the external load L.

Aldrich or Pressure Chemical Co. and used as received. Surfaces were prepared for the adhesion/friction studies either by (1) the "dipping method"—dipping the mica sheets (our supporting substrate surfaces) already glued on silica disks into a pre-filtered (200 nm mesh size) polymer solution in toluene and then lifting them out from the solution at a slow constant speed—or (2) the "casting method"—casting a droplet of the toluene solution on top of each mica surface using a syringe. In both cases, the surfaces are subsequently dried under reduced pressure, using an oil-free vacuum pump, for >10 h to remove the solvent before mounting them into the SFA.

Although the casting method poses no limitation to the thickness of the film that can be prepared, the surfaces of such films are relatively rough. The dipping method, on the other hand, produces smooth films (rms roughness ~0.5 nm).[12] So we used the dipping method for most of our experiments unless we needed to prepare very thick films (many micrometers). The thickness of the films prepared by the dipping method can be controlled (up to 1 μm in the case of high molecular weight PS) by adjusting the concentration of the polymer solution.

The thickness of the polymer films were measured using the optical interference technique of the SFA (employing fringes of equal chromatic order, or FECO) by comparing the fringe positions of the contacting surfaces before and after the polymer layers had been deposited. The standard "symmetric three-layer interferometer equation" was used (mica−polymer−mica) that assumes that the mica sheets and the polymer films on both surfaces have the same thickness. Figure 1 shows the geometry of the surfaces as well as an example of the FECO fringes recorded for two surfaces in adhesive contact.

The FECO fringes of Figure 1 suggest that films have uniform thickness (at the nanoscale over lateral distances of many micrometers) but give no information on their nanoscale roughness. To get this information, we imaged the surfaces by tapping mode AFM. Figure 2 shows AFM images of the three types of surfaces used: untreated, cross-linked and scisssed of high MW PS and PVBC surfaces, showing that in all cases the rms height roughness was below 0.4 nm.

Polydispersity of the Polymers Used. We measured the MW of some of the high MW PS using gel permeation chromatography (GPC) using an Acuflow series II pump equipped with a refractive index detector. Our high MW samples (PS 240 000, 280 000 and 2 000 000) had a high polydispersity index of ~2. In contrast, the low MW samples (PS 1240, 1300, and 2330 Da) had a significantly lower polydispersity index of about 1.1.

Surface Forces Apparatus (SFA) Measurements. We use an SFA (either an SFA III or SFA 2000) for both the adhesion and friction measurements. Details of the designs are described elsewhere.[20,21] Figure 1 shows the different parameters that were measured during routine adhesion and friction experiments. The temperature of the experimental room and apparatus was controlled and monitored to within 0.1 °C in the range 15−35 °C.

Adhesion Measurements. The lower surface is mounted on one end of a double cantilever spring whose spring constant (or stiffness) K_s was calibrated after each experiment (typically K_s = 600 N/m). The base of the spring supporting the lower surface can be raised toward or lowered away from the stationary upper surface. When the two surfaces are in contact, the change in the contact diameter $2r$ as a function of the applied load L can be measured from video recordings of the FECO fringes that image the contact area. The simultaneous recording of r vs L (cf. Figure 1) enables construction of a "JKR plot" for both the loading and unloading branches of an adhesion cycle. Such measurements can be conducted for various contact times, usually by varying the waiting time at the maximum applied load, L_{max}, the end of the loading branch before the start of unloading. At the end of the unloading branch we record the adhesion or "pull-off" force' F_{ad} required to separate the surfaces from adhesive contact by multiplying the jump out distance D_J by the spring constant K_s.

Each JKR plot can be analyzed by fitting the JKR equation[5] to the loading and unloading branches with two fitting parameters, the surface energy γ and the bulk elastic modulus K:

$$r^3 = \frac{R}{K}[L + 6\pi R\gamma + \sqrt{12\pi R\gamma L + (6\pi R\gamma)^2}] \qquad (1)$$

where r is the contact radius, L the applied load, and R the radius of curvature of the (undeformed) surfaces, all of which are directly measured (cf. Figure 1). We assume that the material compressibility modulus K does not change with UV irradiation of the thin polymer films (see below), it being determined mainly by the mica substrate and glue layer between the mica and supporting glass disk.

Alternatively, the surface energy γ can be obtained from the pull-off force F_{ad} using a simpler equation:[5,22]

$$\gamma = F_{ad}/3\pi R \qquad (2)$$

The surface energy deduced from the pull-off force usually coincides with the value fitted to the unloading branch when the latter obeys the JKR equation. This usually occurs when the hysteresis between the loading (advancing) and unloading (receding) energies, γ_A and γ_R, is small. The adhesion hysteresis, defined by

$$\Delta\gamma = (\gamma_R - \gamma_A) \qquad (3)$$

gives the difference in the surface energies of the loading and unloading branches of the JKR plot which is in turn a measure of the energy dissipated during the "adhesion cycle". For smooth surfaces, γ_A is usually insensitive to different surface treatments of the polymer surfaces, and is often closer to the thermodynamic value γ. In such cases, the adhesion hysteresis is mainly determined by γ_R, as deduced from the unloading branch and/or pull-off force. When the adhesion hysteresis is high, the unloading curve can no longer be fitted by the JKR equation, eq 1, and γ_R was then determined from the pull-off force, eq 2.

Friction Measurements. The double cantilever spring supporting the lower surface is mounted on a piezo-electric bimorph slider for friction measurements.[21] The upper surface is mounted on a friction detection device equipped with semiconductor strain gauges that measures the lateral (frictional) force exerted on the upper surface. The sliding speed V and the amplitude of the bimorph slider are controlled by the voltage applied to it by a function generator (Hewlett-Packard, model HP 3325B). A triangular input signal was used to produce a constant sliding velocity in one direction and then back. The range of the sliding amplitude studied was 30 to 220 μm. Both the input voltage to the bimorph slider and the output voltage from the friction detecting device were simultaneously recorded on a chart recorder. The sliding amplitude of the bimorph slider was calibrated using a laser distance detecting device (Keyence model LC-2420, Osaka, Japan). The friction detecting device was also precalibrated by placing

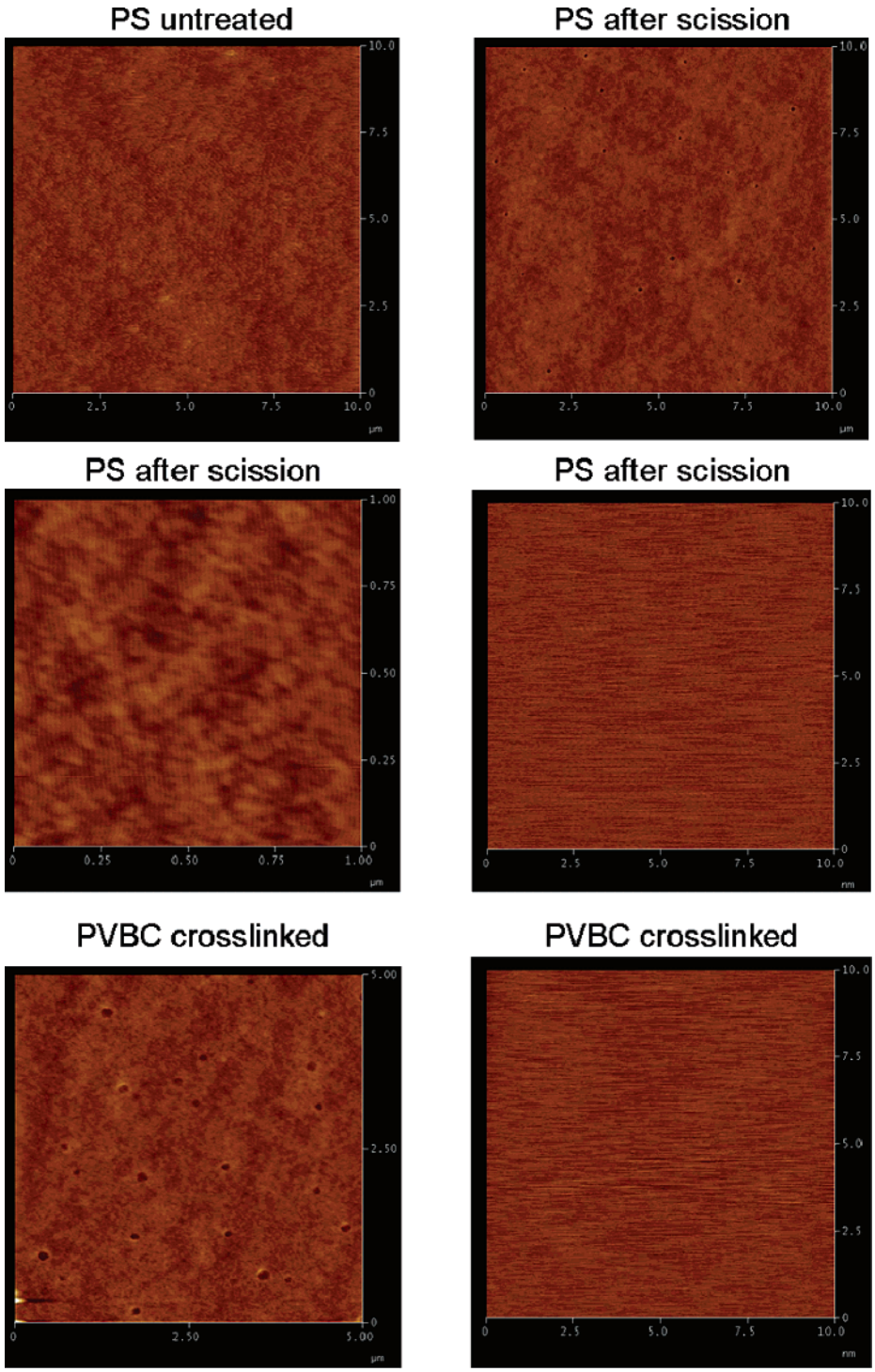

Figure 2. Typical atomic force micrographs of the polymer surfaces: PS (untreated, 10 μm × 10 μm), PS (after scission or "bond broken", 10 μm × 10 μm, 1 μm × 1 μm, 10 nm × 10 nm), PVBC (cross-linked, 5 μm × 5 μm, 10 nm × 10 nm). The untreated polymer surfaces are smooth and featureless whereas small holes may appear after UV treatment for both polymers.

small weights to the sample holder of the vertically held friction device and relating it to the measured output voltage.

Friction forces F were measured (i) as a function of the sliding speed V at constant applied load L and (ii) as a function of the applied load L at constant V. Contrary to the well-known Amonton and Coulomb laws of friction, we found (i) that the friction force F is not simply proportional to the applied load L, and is finite ($F > 0$) even at zero load ($L = 0$), and (ii) that F is not independent of the sliding velocity V nor the contact area πr^2. For these reasons we do not give our friction data in terms of a (constant) friction coefficient $\mu = F/L$.

UV Radiation (Treatment) of Polymer Surfaces. As reported previously,[12] UV radiation of PVBC surfaces in air, i.e., the presence of oxygen *or* nitrogen gas leads to cross-linking of the PVBC chains. In contrast, to cross-link PS, oxygen gas must be rigorously excluded during the UV radiation, otherwise the chains become bond-broken. To cross-link the PS films on the mica surfaces in situ, N_2 gas from liquid nitrogen was first passed through an oxygen purifier (Matheson Tri-gas model 641−02) then fed into the SFA chamber where the UV irradiation was performed using a 46 W UV pen lamp (Pen-Ray 90−0012−01, UVP Inc., Upland, CA). The distance of the polymer surfaces from the UV source was approximately 1 cm. The temperature rise due to UV radiation was a few degrees at most (even after prolonged radiation), and was considered to be unimportant. For both

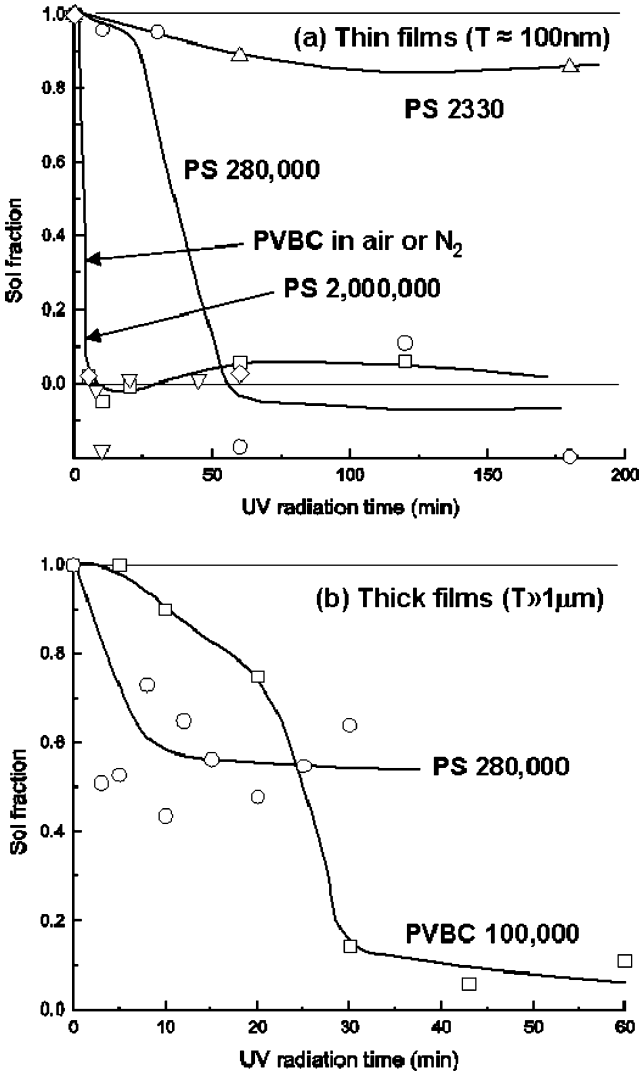

Figure 3. Sol fraction of PS and PVBC surfaces is shown as a function of UV radiation time: (a) thin (≈100 nm) PS and PVBC films in different atmospheres measured using ellipsometry and (b) thick (≫ 1 μm) PS and PVBC films measured using microbalance. The UV radiation was carried out in oxygen-free nitrogen atmosphere for PS films, and both in air and in nitrogen for PVBC films. We typically waited for 20 min to determine the "sol fraction" dissolved, although equilibrium was generally achieved within 1 min or less for both polymers. Sol fraction apparently depends on the thickness of the polymer films, especially for PS, presumably because the penetration depth of the UV light limits the maximum thickness of the films that can be cross-linked. It appears that both thick and thin PVBC films can be eventually cross-linked, either in nitrogen or in air. For thin PS films, the sol fraction of MW 2 000 000 drops more readily than that of MW 280 000 and the sol fraction of MW 2330 does not appear to go down very much, indicating that the higher the molecular weight PS it is easier to cross-link. The errors were roughly the size of the data points for each experiment, but the scatter between different experiments was larger, especially for the thicker films, as in part b.

types of UV treatments the chamber was flushed for 15−20 min with either inert nitrogen gas or dry air (oxygen gas) prior to the UV treatment, during the treatment, and for 15−20 min after the UV source was turned off to ensure that all the free radicals have disappeared.

Sol Fraction Measurements. To estimate the extent of cross-linking as a function of UV radiation time under a given condition, we carried out a series of sol fraction measurements (Figure 3). PS or PVBC films deposited on freshly cleaved mica sheets or silicon wafers are mounted in the SFA chamber after the initial amount of the polymer film was measured either by microbalance or elipsometry. After the UV treatment, each sample was immersed in toluene to dissolve the remaining monomers and then dried under reduced pressure. The amount of the film remaining on the substrate was then measured, again by a microbalance or ellipsometry, which gives the amount of polymer that went into the solution (the "sol fraction") as well as the cross-linked fraction of the original film.

The sol fraction of a given polymer for a given UV radiation time apparently depends on the initial thickness of the polymer films as well as on the precise position of the sample in the SFA with respect to that of the UV light source (the distance and the angle). In addition, the cross-linked polymer films are known to swell in toluene and the toluene in the cross-linked network might remain trapped after our drying procedure, resulting in the (apparently unphysical) negative sol fraction (the thickness increases after the extraction). Clearly our sol fraction data are not useful for rigorous quantitative analysis. Here we merely note from Figure 3 that (1) the sol fraction decreases as the UV radiation time is increased, (2) as expected, the probability of cross-linkling a PS molecule to its neighbors is higher the higher its MW, and (3) PVBC can be cross-linked equally well in nitrogen or in air.

Table 1. Molecular Weights (MW) and T_g Values[a] of the PS Studied

classification	high MW			low MW		
MW (Da)	2 000 000	280 000	240 000	2330	1300	1240
T_g (°C)	107	106	106	69	39	35

[a] The T_g values refer to the bulk materials. T_g is not well-defined in thin films or near surfaces and almost certainly varies as one moves from the surface into the film. We discuss this matter in more detail, as it pertains to our experiments, in a forthcoming paper.

Results

In all, about 30 separate experiments (not all successful) and samples were tested, in which each experiment involved three to eight different surface "positions".

We studied only one MW for PVBC (100 000 Da).[29] For PS, we studied a series of weight-average MWs of 1240, 1300, 2330, 240 000, 280 000 and 2 000 000.[2] On the basis of our results, to be described below, we classify our PS into two groups: low MW (1240−2330 Da), and high MW (240 000−2 000 000 Da). The glass transition temperature, T_g, of each PS was estimated using the Fox−Flory equation.[23] T_g estimates are summarized in Table 1. The T_g values of some of the samples PS were also measured by differential scanning calorimetry (DSC) and found to agree well with the calculated values listed in Table 1. The T_g of PVBC 100 000 was also measured by DSC and found to be 70 °C.

Adhesion and Friction of Untreated and Cross-Linked High MW Polymers. For the untreated (used as deposited) PS and PVBC, their adhesion hysteresis and friction exhibited qualitatively similar behavior and trends: the adhesion hysteresis is small and does not increase much with contact time. The cross-linked polymers exhibited comparable adhesion hysteresis, while the bond-broken polymers had much larger hysteresis that was also contact time-dependent. Examples of JKR plots for PS 2 000 000 are given in Figure 4. The results are similar to those for two PVBC surfaces as previously reported.[12] The contact-time dependence of the receding adhesion forces (on pull-off) for the two highest MW PS surfaces before and after scission are shown in Figure 5.

The friction forces correlated with, and were much more sensitive to the different surface treatments than,

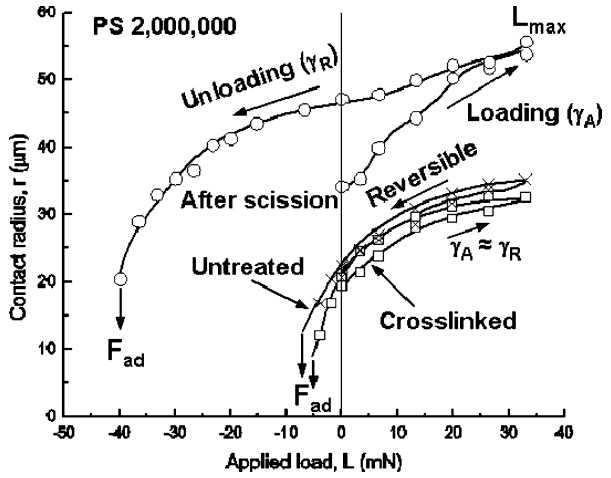

Figure 4. Typical JKR plot of PS 2 000 000 surfaces that are untreated, that are cross-linked and that are observed after scission. Both untreated and cross-linked surfaces exhibit small adhesion hysteresis. After scission the adhesion hysteresis is significantly larger and the unloading curve can no longer be fitted by the JKR equation, eq 1. γ_R was then determined from the pull-off force, eq 2. Errors are roughly the size of the data points.

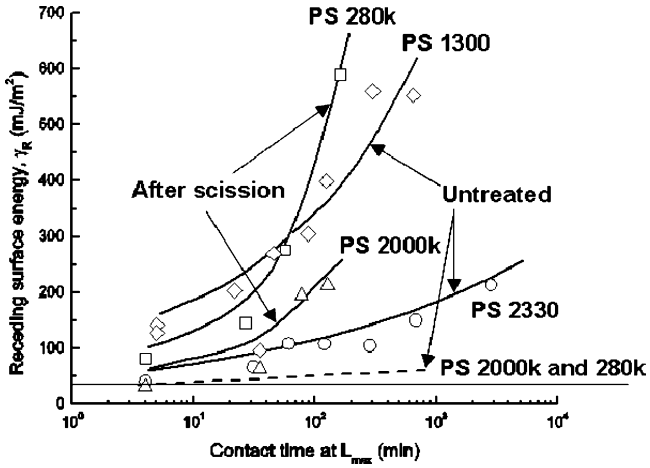

Figure 5. Adhesion hysteresis of untreated PS 2330 surfaces, untreated PS 1300 surfaces, PS 280 000 surfaces after scission (14 h UV radiation), and PS 2 000 000 surfaces after scission (16 h UV radiation) are plotted as a function of contact time. The contact time was measured when the surfaces were compressed at the maximum loads. The thin horizontal line at $\gamma = 45$ mJ/m^2 corresponds to the thermodynamic surface energy.

the adhesion hysteresis (a semiquantitative comparison between the measured friction and adhesion hysteresis based on a simple model is done and further discussed in the Discussion). Figure 6 shows some typical friction traces for high MW untreated PS (PVBC traces were qualitatively similar). When the surfaces are slid slowly a stiction spike F_{st} is followed by decaying stick−slip motion (Figure 6a), where the stick maxima or "static friction" F_s and the slip minima or "kinetic friction" F_k approach each other as the stick−slip motion proceeds. At higher sliding speeds (Figure 6b) the stick−slip amplitude decreases, the frequency increases, the decay is faster, and F_s and F_k merge within a few stick−slip spikes resulting in smooth sliding. At even higher sliding speeds, above the so-called critical velocity V_c (Figure 6c), only smooth sliding, with or without a small stiction spike, occurs.

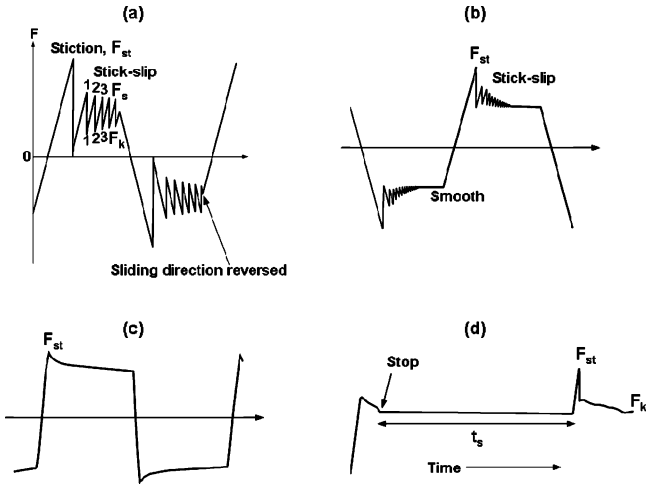

Figure 6. Typical friction force profiles observed between high MW untreated polymer surfaces. (a) Decaying stick−slip motion is typically observed at slow sliding speeds and/or large external loads. (b) Such decaying stick−slip motion may merge into a continuous smooth sliding motion for sufficiently high sliding speeds. (c) Only smooth sliding may appear for even higher sliding speeds. (d) Stiction spikes are observed for stop−start experiments when the stopping time is sufficiently long.

Figure 6d shows an example of a 'stop−start measurement', used to estimate the relaxation time for the surfaces to make the transition from their smooth, dynamic sliding state where $F = F_k$ to the larger static or stiction state where $F = F_{st}$, when sliding motion is resumed at the same V after a certain stopping time, t_s.

The speed dependence of the friction forces $F(t)$ for both untreated and cross-linked high MW PS at zero load ($L = 0$) is summarized in Figure 7. Very similar trends were obtained for PVBC 100 000, as shown in Figure 8. We note that for both systems there is a critical velocity V_c above which the stick−slip disappears to be replaced by smooth sliding.[30] Stick−slip is often a manifestation of the interfacial friction force decreasing with V, which is equivalent to the effective thin film viscosity decreasing faster than $1/V$ and/or to a maximum in the shear stress, which gives rise to saw-tooth instabilities over a certain velocity regime. Similar effects also occur in certain *bulk* complex fluid systems. The critical velocity V_c is believed to be related to the characteristic length δ and relaxation time τ_c of the energy-dissipating mechanism via the relation: $V_c = \delta/\tau_c$. In this case, putting $\delta \sim 1-2$ nm (see Discussion) and the measured $V_c \sim 1$ μm/s, we obtain a relaxation time of $\tau_c \sim 1-2$ ms for the loops to entangle/disentangle across the shearing interfaces (under a finite load and confinement).

We also studied the load dependence of the friction forces $F(L)$ at various sliding speeds V. A few examples are shown for PS 2 000 000 in Figure 9 and for PVBC 100 000 in Figure 10. The results show that the friction forces increase quasi-linearly with the applied load although the friction is clearly finite at zero and even at small negative loads due to the adhesion between the surfaces. PVBC shows little zero-load friction, and a straighter line for F *vs* L (following Amontons' law), as expected for low adhesion surfaces. PS shows a more curved line and a large finite friction at $L = 0$, also as expected. These curves can be fitted to a JKR superimposed on an Amontons equation to extract important molecular-scale information and parameters for both

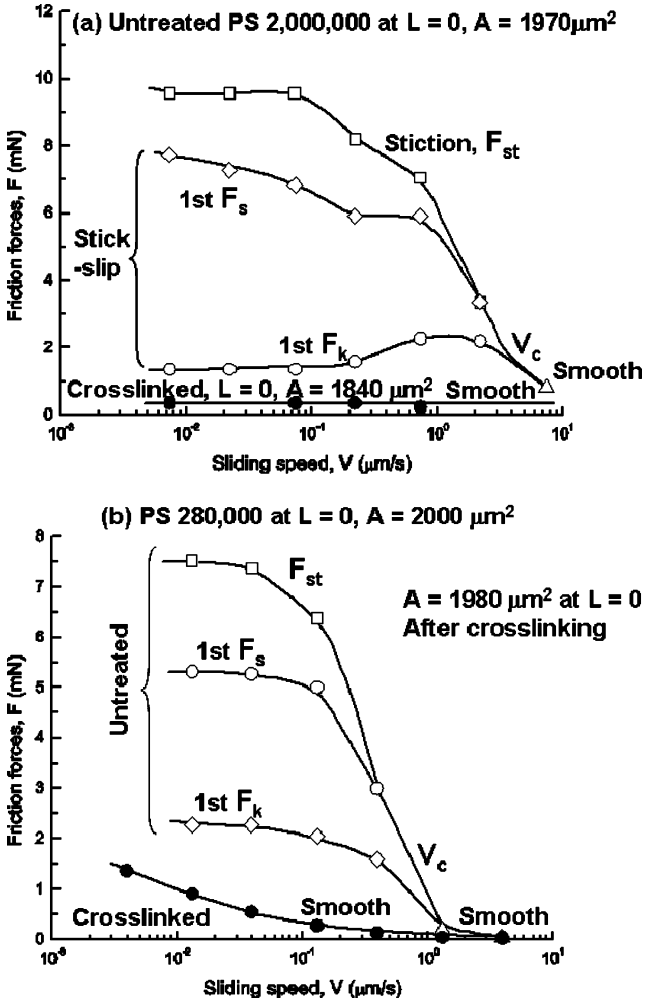

Figure 7. (a) Friction forces between two PS 2 000 000 surfaces before and after cross-linking as a function of sliding speed. (b) Friction forces between two PS 280 000 surfaces before and after cross-linking as a function of sliding speed. The results are similar to those between two PS 2 000 000 surfaces.

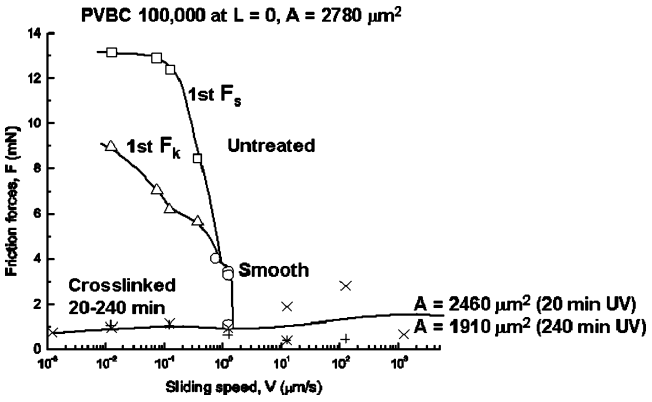

Figure 8. Friction forces between two PVBC surfaces before and after cross-linking as a function of sliding speed. Two sets of data that correspond to different UV radiation time (extent of cross-linking) are shown for the cross-linked surfaces. There is little difference between the cross-linked pairs suggesting that once a certain fraction of the polymer films is cross-linked further UV treatment makes little difference to the friction between such polymer films.

systems (see Analysis and Discussion). Figure 10 shows that only smooth sliding occurs at low loads for sufficiently high sliding speeds. However, even at high V, it is possible to induce stick−slip motion by increasing

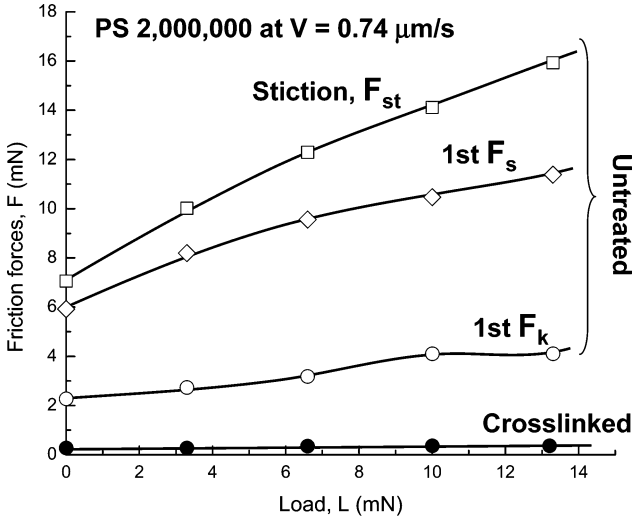

Figure 9. Friction forces between two PS 2 000 000 surfaces before and after cross-linking as a function of applied load. The friction forces of untreated surfaces are not linear with the applied load and clearly finite (nonzero) at zero external load, indicating the Amonton's law does not hold here. The untreated surfaces exhibit stick−slip motion at all loads studied (for $V = 0.74$ μm/s). After cross-linking the stick−slip motion disappears and only small smooth sliding appears at all loads. For the untreated surfaces the contact area increased from ~2000 to ~3100 μm^2 as the load increased from zero to ~13 mN, while for the cross-linked surfaces it increased from ~1800 to ~3600 μm^2 over the same range of loads.

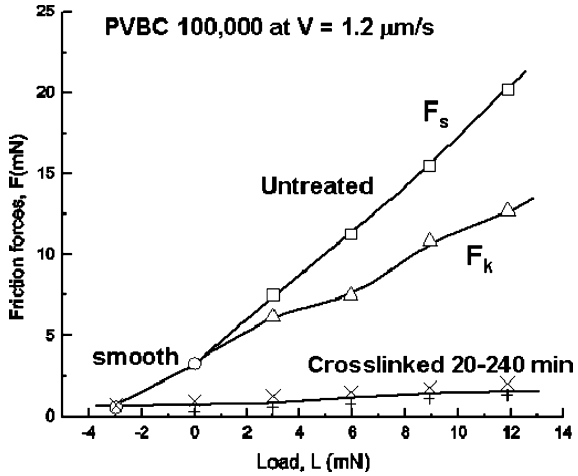

Figure 10. Friction forces between two PVBC 100 000 surfaces before and after cross-linking as a function of applied load. The friction forces of untreated surfaces are more linear with the applied load compared to that of PS (quasi-Amontons), although the friction forces are clearly finite (nonzero) at zero external load. For $V = 1.2$ μm/s, the untreated surfaces exhibit smooth sliding at low loads ($L \leq 0$ mN) but stick−slip motion at higher loads ($L \geq 3$ mN). After cross-linking the stick−slip motion disappears and only small smooth sliding appears at all loads, and the friction forces are similar to those that have been cross-linked for different UV irradiation times. For the untreated surfaces the contact area increased from ~1700 to ~4500 μm^2 as the load increased from zero to ~12 mN, while for the surfaces that had been cross-linked for 20 min it increased from ~1500 to ~4500 μm^2 over the same range of loads, and from ~1400 to ~3300 μm^2 for surfaces that had been cross-linked for 240 min.

L, where the amplitude $\Delta F = F_s - F_k$ of the stick−slip increases with further increasing in L above the critical load L_c.

Stop−start experiments (cf. Figure 6d) were carried out at a sufficiently high sliding speeds ($V > V_c$) where

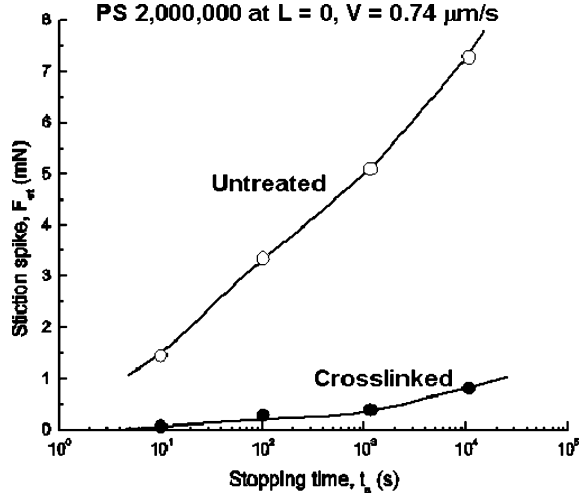

Figure 11. The height of the stiction spike, F_{st}, of PS 2 000 000 in stop−start experiments is shown as a function of stopping time, t_s. The stiction spike of untreated surfaces increases sharply with the stopping time whereas that of cross-linked pair remains low.

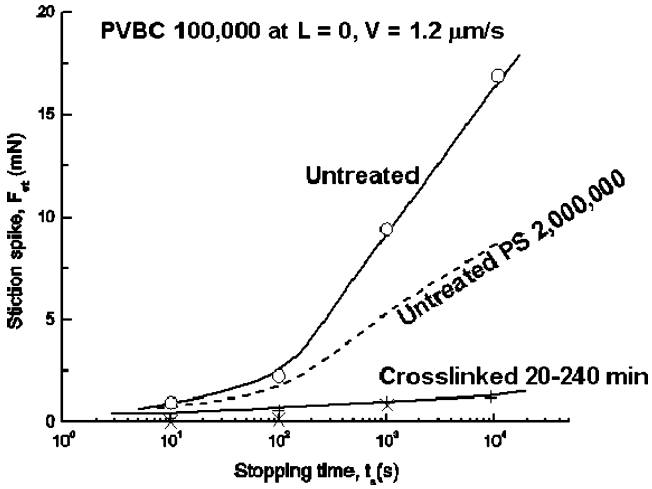

Figure 12. Height of the stiction spike, F_{st}, of PVBC 100 000 in stop−start experiment shown as a function of stopping time. The stiction spike of untreated surfaces increases sharply with the stopping time whereas that of cross-linked pair remains low. Once again, there is little difference between the pairs cross-linked for different UV irradiation times.

the steady-state sliding is smooth. The results show that the stiction spike heights F_{st} increase with the stopping times t_s for both PS (Figure 11) and PVBC (Figures 12), both measured at zero load. If the untreated surfaces are kept in prolonged contact, the contact area increases by up to double the initial area due to flow of polymer into the bifurcation zone (this does not occur with the more elastic cross-linked polymers). Thus, the roughly order of magnitude increase in the stiction forces after prolonged contact shown in Figures 11 and 12 cannot be attributed to deformation.[31]

When the high MW polymers are cross-linked, the friction forces dropped dramatically and only smooth sliding occurred at all the sliding speeds (0.001−1000 μm/s), loads (0−15 mN), pressures (0−6 MPa) and stopping times ($10-10^4$ s) studied, as shown in Figures 7−12.

We also measured the effect of UV irradiation time on PVBC surfaces, which gave different sol fractions and cross-linking densities (Figure 3). Figures 8, 10, and 12 show that the friction forces measured at different speeds, loads or stopping times are very similar for PVBC surfaces after two quite different UV radiation times, 20 and 240 min. Presumably, the cross-linking proceeds from the top surface of the film toward the inner part, and the outermost layer is already fully cross-linked once the overall sol fraction falls below 75% (>25% of the film is cross-linked).

Figures 8 and 10 show that at high sliding velocities $V > V_c$ and low loads $L < L_c$ the untreated surfaces of PVBC exhibit smooth sliding and the friction forces are as small as for the cross-linked surfaces. However, for the untreated surfaces the friction forces increase steadily as the load is increased and more abruptly as the velocity is decreased, with the further appearance of stick−slip motion. In contrast, for the cross-linked surfaces the friction forces remain smooth and low as L increases or as V decreases.

Adhesion and Friction of Bond-Broken High MW Polymer (PS). It has been reported that in situ chain scission of PS surfaces is readily achieved by UV radiation in air. We did not characterize the extent of the chain scission (number of chain ends per unit area) for a given UV radiation time in air. We carried out chain scission only for PS surfaces that were first cross-linked (and after their adhesion and friction forces were measured).

As we reported previously,[12] and now shown in Figures 4, 5, 13, and 14 in more detail, both the adhesion hysteresis and friction forces of PS increase with the UV radiation time in air, and stop−start experiments (results not shown) show that the stiction spikes also increase sharply with the radiation time. For short radiation times, both the adhesion hysteresis and friction forces are still quantitatively measurable; but after prolonged UV radiation, the friction forces become so large that the surfaces no longer slide, but remain stuck or become damaged. For these situations only the adhesion hysteresis is still measured (Figure 4) although the shapes of the deformed surfaces no longer follow the JKR geometry, for example, separation now occurs at a smaller "contact radius" r than predicted by the JKR theory. For bond-broken surfaces the adhesion hysteresis strongly depends on the loading and unloading rates and on the contact times at different loads. This effect can be quantified in a number of ways; here we choose to do this by measuring the unloading (receding) surface energy γ_R as a function of the contact time at maximum load $L = L_{max}$ (Figures 4 and 5).[32]

In general, three trends could be distinguished for the bond-broken surfaces: (1) The longer the contact time the larger the adhesion hysteresis (for the same loading-unloading rates); (2) bond-broken surfaces exhibited much larger hysteresis than the untreated and cross-linked surfaces; (3) the lower the MW, the higher was the hysteresis (Figure 5).

When the adhesion energy became very high, as occurred for bond-broken PS, separation from contact causes irreversible damage. By damage we mean that the surfaces no longer separate or peel away "cleanly" along the smooth, well-defined interface that they followed on loading. After damage it was impossible to repeat the JKR measurement at the same "contact position": after each separation one must find a new contact position to obtain reproducible results.

Adhesion and Friction of Untreated Low MW Polymer (PS). Since low MW PS cannot be easily cross-linked (Figure 3a), we describe our results only with

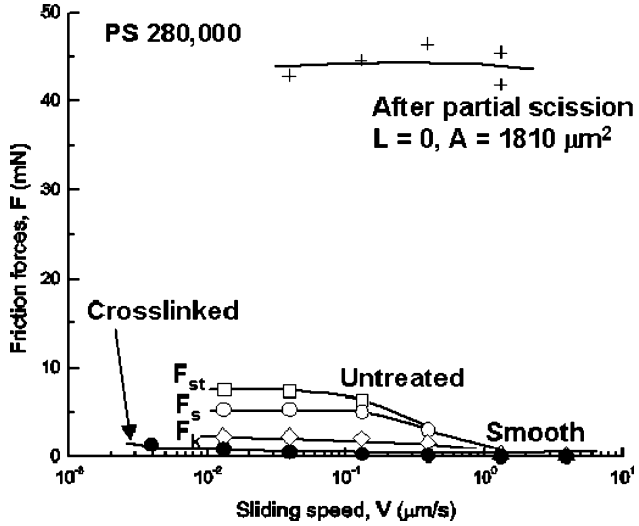

Figure 13. Friction forces between two PS 280 000 surfaces after moderate scission as a function of sliding speed, V. For comparison, the data of untreated and cross-linked surfaces are also shown. The friction forces increase dramatically. With further UV irradiation (scission) the friction forces becomes so large that the surfaces remain stuck even driven with the maximum amplitude (130 μm).

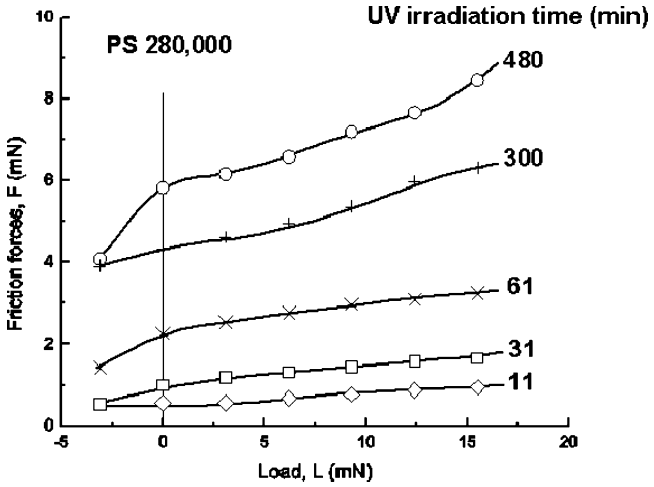

Figure 14. Friction forces between two PS 280 000 surfaces go up as the chain scission proceeds (as the UV radiation time increases). With further UV irradiation the friction forces becomes so large that the surfaces remain stuck even driven with the maximum amplitude (130 μm). For the surfaces that had been radiated for 31 min the contact area increased from ~2200 to ~3400 μm^2 as the load increased from zero to 16 mN.

untreated PS. The friction forces for these surfaces were very high and difficult to measure accurately because the surfaces were irreversibly damaged as soon as sliding commenced. However, the adhesion hysteresis of untreated PS was accurately measurable. Figure 15 shows several typical JKR plots for two PS 2330 surfaces, showing an increased hysteresis with contact time t. The data are rearranged in Figure 5 to show several receding surface energies γ_R as a function of the contact time.

As can be seen in Figure 5, the adhesion hysteresis of *untreated, low* MW PS is large and comparable to that of *bond-broken, high* MW PS surfaces, and both increase sharply with the contact time. The adhesion hysteresis becomes even larger as the molecular weight is further decreased from 2330 to 1300 to 1240 (and even to lower MW). To see a systematic trend among these different

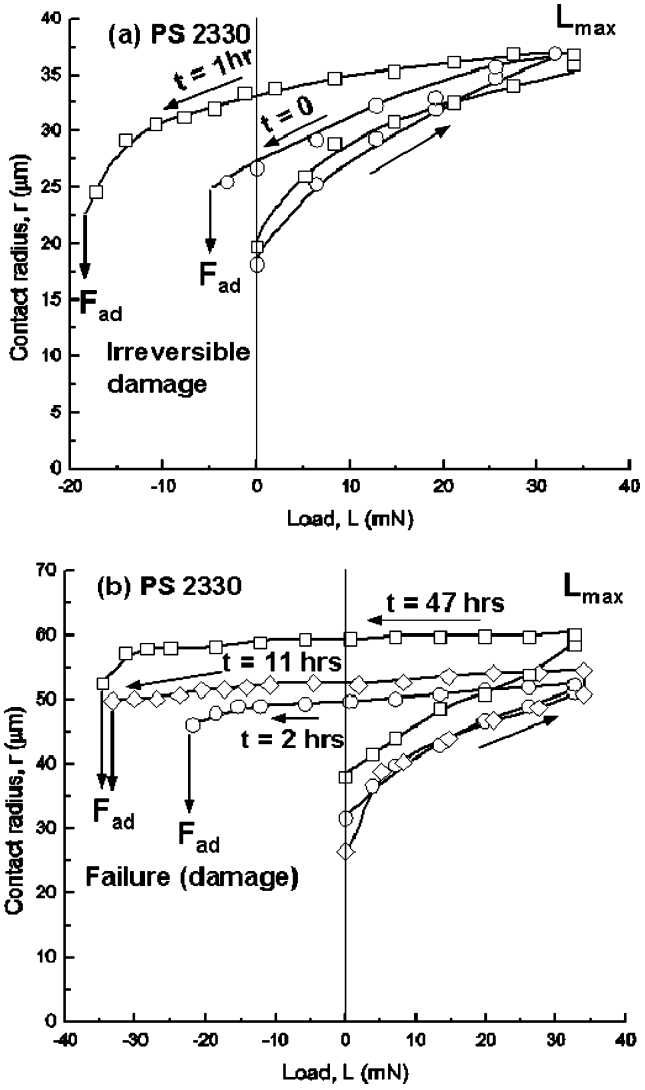

Figure 15. Typical JKR plot of untreated PS 2330 surfaces for different contact times. For clarity we split the data into two panels (a) for shorter contact times and (b) for longer contact times. Errors are roughly the size of the data points.

molecular weights, we plot in Figure 16 the adhesion hysteresis as a function of the molecular weight of the PS at two different contact times. The deformations of the surfaces upon prolonged contact, indicated by a steady increase in the contact radius r at constant load, was larger for the lower molecular weight PS, presumably due to the decreased T_g (and, therefore, increasing viscous component) of these polymers (see Figure 3 in ref 9). As already mentioned, an increased contact area should contribute further to the increase of the receding adhesion force and hysteresis, i.e., in addition to the contribution from the interdiffusion of chains across the interface.

As for the *bond-broken high* MW PS surfaces, it was difficult to repeat the adhesion measurements of *untreated low* MW PS at the same contact position because of the damage caused on separation, especially after longer contact times. Nevertheless, measurements repeated at different contact positions on the same pair of surfaces showed consistent results.

Asymmetric Surfaces. Two such systems were studied. In the first, the adhesion of a cross-linked (low adhesion, low friction) surface of PS 240 000 and a bond-broken (high adhesion, high friction) surface of PS

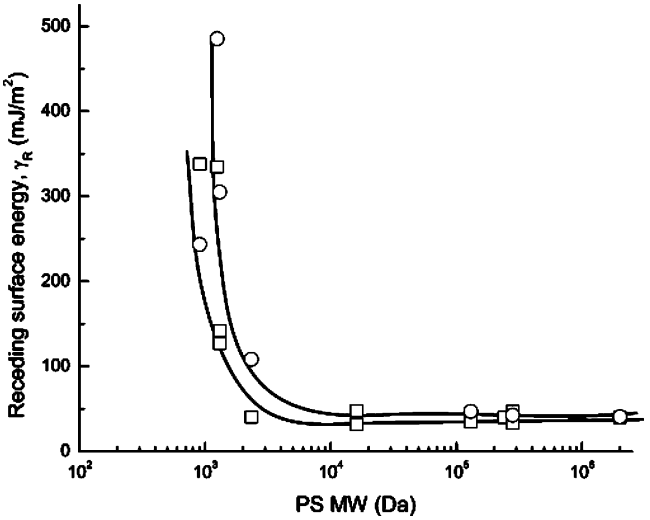

Figure 16. Adhesion hysteresis between two untreated PS surfaces of various molecular weights is shown for two different contact times. Formation of meniscus is observed around the contact area that grows with contact time. The growth rate of the meniscus is larger for the surfaces of lower molecular weight, resulting in a larger contact area after a given time of contact. Such increased contact area clearly contributes to the increase of the adhesion hysteresis.

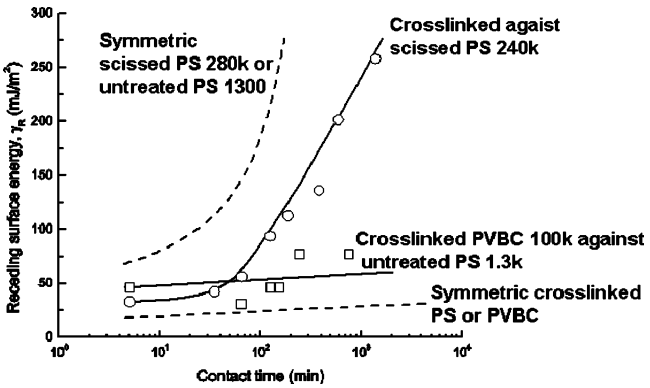

Figure 17. Adhesion hysteresis is measured between asymmetric pairs. Adhesion hysteresis of cross-linked against bond-broken PS 240 000 surfaces is larger than that between two cross-linked or untreated PS 240 000 surfaces but smaller than that of two bond-broken PS 240 000 surfaces. Adhesion hysteresis of cross-linked PVBC 100 000 against untreated PS 1300 surfaces is larger than that between two cross-linked or untreated PVBC 100 000 surfaces but smaller than that of two untreated PS 1300 surfaces.

240 000 (the same MW) was measured (Figure 17). The receding surface energy of the asymmetric pair was found to be intermediate between those of the symmetric surfaces. The friction forces were high and difficult to measure due to damage.

In the second system, both adhesion and friction were measured between a highly cross-linked surface of PVBC 100 000 and an untreated surface of PS 1300. Here, too, we have two very different surfaces, but now a *high MW cross-linked* one (of low adhesion and friction) against a *low MW untreated* one (of high adhesion and friction). Again, the receding surface energy of the asymmetric pair is intermediate between the two symmetrical surfaces (Figure 17). The friction forces for these asymmetric surfaces showed stick−slip motion at all the speeds studied (Figure 18); in contrast, those between the two symmetric cross-linked PVBC 100 000 surfaces were smooth (and small), while those

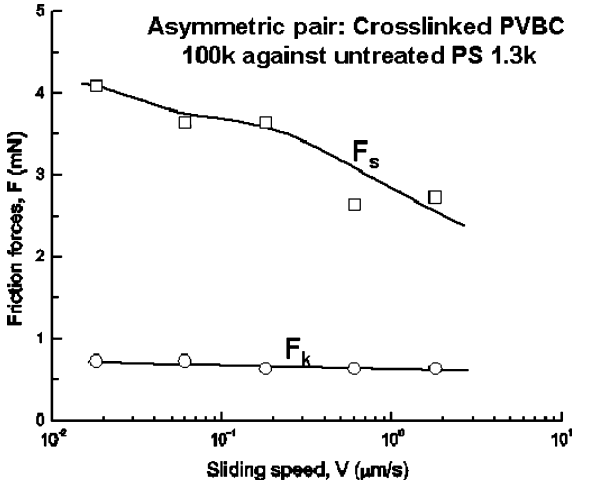

Figure 18. Friction forces are measured for an asymmetric pair or cross-linked PVBC 100 000 against untreated PS 1300 surfaces at $L = 0$. Stick−slip motion is observed at all sliding speeds. The friction forces between two cross-linked PVBC surfaces (not shown) are smooth and small at all sliding speeds, while those between two untreated PS 1300 surfaces were difficult to measure because the surfaces got damaged very easily.

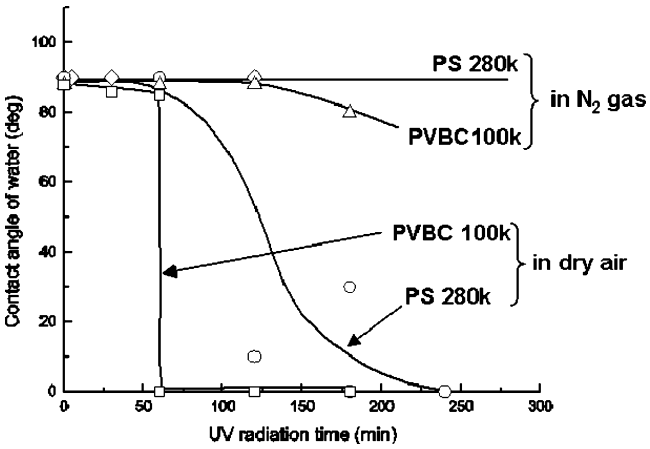

Figure 19. Contact angles of water on PS and PVBC surfaces that are treated by UV for different radiation times. The contact angle is high for both polymers prior to the UV treatment, suggesting that the polarity of PVBC is similar to that of PS. The contact angle remains high for both polymers even after the UV treatment in an oxygen-free nitrogen atmosphere, suggesting that the polymer surfaces remain nonpolar. In contrast, the contact angle drops to almost zero for both polymers when UV treated in air for sufficiently long time, suggesting that the surfaces become highly polar (hydrophilic).

between the two symmetric untreated PS 1300 surfaces were high and difficult to measure due to damage.

Effect of Polar Groups. When the polymer surfaces are radiated by UV in air to achieve scission of PS or cross-linking of PVBC, there may also be a change in surface chemistry.[18,19] The significant changes observed in the adhesion and friction following UV treatment could therefore be attributed to the change in the chemical nature or polarity of the exposed surface groups. To examine this, we first carried out water contact angle measurements to measure the changes in the polarity of PS and PVBC surfaces that had been irradiated for different times in air (Figure 19). The results were also compared to contact angle measurements on UV treated surfaces in an atmosphere of oxygen-free nitrogen gas.

We found several interesting features. First, the quasi-static advancing contact angles (measured after the macroscopic three-phase contact line stopped moving) were high for both polymers prior to the UV treatment. In our previous report,[12] we assumed that since the $-CH_2Cl$ group in each segment of PVBC is polar, the PVBC surface should be more polar than the PS surface. However, the equally high contact angle of water on both surfaces suggests that the polarity (or nonpolarity) of the submolecular groups exposed at a PVBC surface are similar to those exposed at a PS surface. It is likely that the polar $-CH_2Cl$ groups of PVBC are facing into or buried under the surface which exposes only the lower-energy, nonpolar $-CH_2-CH-$ groups of the PVBC segments.

Second, the contact angle remains high for both polymers even after the UV treatment in an oxygen-free nitrogen atmosphere. Third, the contact angle drops to almost zero for both polymers after UV treated in air for a sufficiently long time, indicating that the surfaces eventually become highly polar/hydrophilic (see XPS results below). Fourth, the hydrophobic-to-hydrophilic transition occurs at different UV irradiation times for PS and PVBC, and appears to be fairly abrupt for PVBC 100 000 suggestive of a structural transition at the surface for this polymer. We note that the lack of a direct correlation between the contact angle θ and adhesion energies γ_{SV} is because they measure quite different parameters, as shown by the Young equation:

$$\gamma_{SV} = \gamma_{SL} + \gamma_{LV} \cos \theta$$

In an attempt to determine the chemical structure of the oxygen containing groups on the surface after the UV treatment we tried to characterize the surfaces using X-ray photospectroscopy (XPS). However, the XPS spectra showed a superposition of many different peaks which were difficult to deconvolute. We did note, however, that the UV treated surfaces appeared to contain a wide range of different oxygen containing groups including C=O, C−O−, C−O−O−, C−OH, and COOH (water and CO_2 may come in during the UV radiation in air). We also attempted to characterize the oxidized surface layer using neutron reflectometry. The results (not shown) could not identify the chemical structure of the oxidized surface layer, but did show gradual growth of the thickness of the layer as the UV irradiation time is increased. Thus, it is reasonable to conclude that the effect of the UV treatment proceeds from the very top layer to the inner part of the polymer films.

Discussion

Importance of Chain Ends on Adhesion and Adhesion Hysteresis. Our results strongly suggest that the number of short[33] chain ends exposed on a polymer surface, and the mechanism by which these penetrate an opposing surface, are the most important factors that determine the adhesion hysteresis and friction forces between two polymer surfaces. We also reaffirm previous findings that adhesion energy hysteresis (essentially the "receding", "pull-off", or "separation" energy[34]) and friction are intimately related, which is further analyzed at the end of this Discussion. Our main conclusions are illustrated schematically in Figure 20. We first will discuss the adhesion results of our untreated polymers.

The JKR plots of the untreated low MW PS surfaces exhibited the most hysteretic, i.e., irreversible, behavior (Figures 15). It is clear that the JKR equation, eq 1, cannot be fitted to the unloading branches in such situations. However, if the surface energy determined from the experimental pull-off force using eq 2 remains valid,[35] we can draw several conclusions from our data. Our results show that once the MW of untreated PS falls below 10 kDa the adhesion hysteresis increases sharply. This would be difficult to explain if the adhesion hysteresis is to be attributed to the interpenetration of polymer loops, because there should be fewer loops at the surfaces as the density of ends increases. Although interpenetration of polymer loops may be occurring, its effect on adhesion hysteresis appears to be minor compared to that of chain ends. The mechanism of chain end penetration and its contribution to adhesion hysteresis may be expected to be determined by a combination of (1) the number of the chain ends at the surfaces per unit area, (2) the "real" area of contact,[36] and (3) the (thermally activated) rate of interpenetration of chain ends into the opposing surface and the extent (depth) of the interpenetration.

The number of the chain ends at the surfaces per unit area is expected to increase as the molecular weight of the polymer decreases. The "real" contact area is expected to be larger the softer it is, i.e., the lower is its bulk elastic and viscoelastic moduli, due to the ease with which the surface asperities can locally flatten. This effect is expected to increase with decreasing MW as the T_g of the polymer is approached. The real contact area is also expected to be initially higher the smoother the surfaces. The mobility and interpenetration rate of chain ends is also expected to increase as the molecular weight is lowered and its T_g decreases to approach the experimental temperature. Concerning the interpenetration depth, we note that the largest effects were observed for the lowest MW PS 1240 used in this study. Since PS 1240 has only 12 segments of fully extended length $(12 - 1) \times 0.25 + 2 \times 0.23 \approx 3.25$ nm, a maximum of six segments of "interpenetration" length $\delta \sim 1.6$ nm can enter each surface (and still have the same length of segments within the other surface), giving us an indication of how few interpenetrating segments and interpenetration length are needed to produce very large adhesion hysteresis (and friction) forces. This illustrated schematically in Figure 20.

The above conclusions regarding the overriding importance of chain ends are supported by our studies with surfaces where chain ends were produced by scission. Thus, the most hysteretic surfaces were those that were subjected to cross-linking followed by scission − the hysteresis increasing with the UV irradiation time that could be correlated with the generation of "ends" rather than loops or other chemical species at the surfaces.

Importance of Chain Ends on Friction Forces. The observed reduction of the friction forces between high MW polymer surfaces after cross-linking may also be explained in terms of the reduced number of "free" or mobile chain ends at the surfaces (even if their number density may not change). Cross-linking could also prevent chain ends from penetrating into a surface that exposes a semirigid network of cross-linked segments. As previously noted,[12] friction forces are generally much more sensitive to changes in interfacial structure and interactions than adhesion forces or adhesion hysteresis. Thus, the relatively large effect of

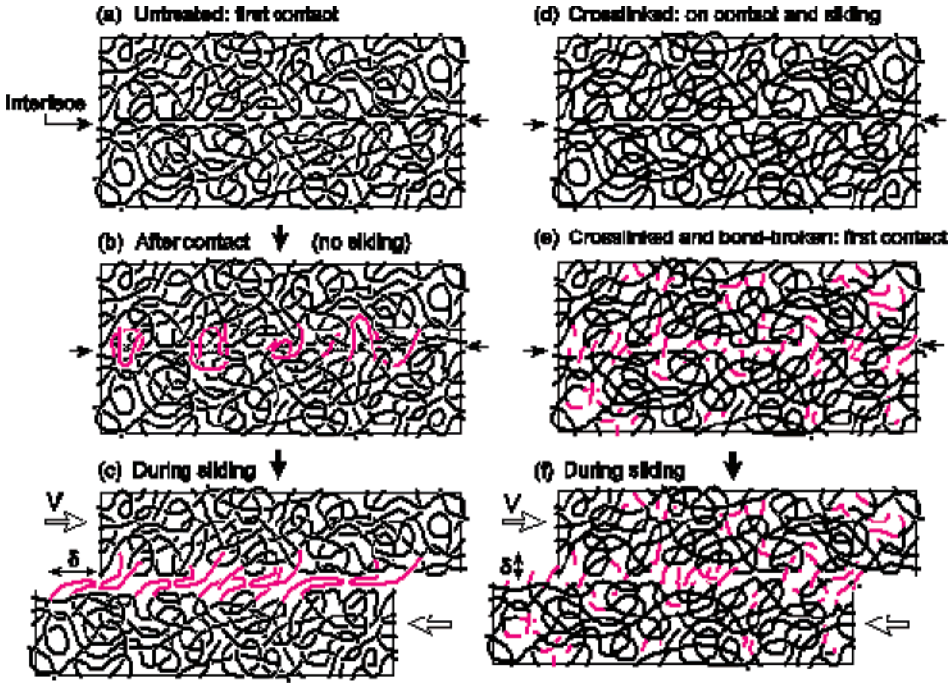

Figure 20. Schematic figure that summarizes our results regarding the different configurations of polymer chains at a polymer−polymer junction under static and sliding conditions. (a) Untreated high MW polymer surfaces in initial contact, showing few ends in the bulk and at the interface. (b) Untreated surfaces of part a after a short time in contact: some loops and ends have diffused away from their initial positions (dotted lines) and penetrated into the opposite surface (red lines). (c) Surface on sliding at low velocities V, where the loops have sufficient time to interpenetrate across the interface (not shown), but at high V they do not, becoming shear-aligned as shown by the red lines, resulting in lower friction. The ends, however, being more mobile, can interpenetrate even at high V, as shown. (d) Configuration of cross-linked surfaces on initial contact, which does not change with time or sliding (not shown), resulting in low adhesion hysteresis and friction that are largely independent of the contact time or sliding speed. Note the higher density of cross-links closer to the polymer surfaces. (e) Cross-linked polymer surfaces of part d after scission brought into contact where interpenetration of the ends (red lines) has occurred rapidly due to their high mobility. We show ends interpenetrating with opposite ends as well as penetrating into opposite cross-linked regions ("asymmetrical" case). (f) Inter-penetration of ends during sliding, which even at high V, is essentially the same as at rest due to their high mobility, resulting in high friction at all sliding speeds. The length of interpenetrating segments, denoted by δ and estimated to be 1−2 nm (see text), is assumed to be similar for loops and ends. Errors are roughly the size of the data points.

cross-linking on the friction forces of both PS and PVBC (Figures 7−12) were apparently not large enough to show up in the adhesion hysteresis (Figure 4). However, the much larger effects of scission (UV irradiation time) were clearly seen in both the adhesion hysteresis and friction data.

The decaying stick slip behavior that was observed after each reversal of the sliding direction between untreated high MW polymer surfaces at slow sliding speeds has not been previously observed with other systems, which tend to show regular (periodic) stick−slip, chaotic stick−slip or no stick−slip, but not a steadily decreasing regular stick−slip.[24,25] The decaying stick−slip may reflect changes associated with the ordering and reordering of chain ends at the shearing interfaces during sliding reversals. Thus, after each reversal, the surfaces remain in stationary contact for a certain period of time, allowing the interpenetration of the polymer chains across the contacting interface, thereby increasing the critical shear stress required for the resumption of sliding is (the stiction spike). The stiction spikes were indeed found to be smaller at higher sliding speeds (Figures 7 and 8) which result in shorter contact times after each reversal of the sliding direction.

On resumption of sliding, each stiction spike is followed by stick−slip sliding, indicative of (i) repenetration of the ends after each slip, (ii) solidlike to liquidlike transitions of the ends, or (iii) a monotonic decrease in the friction force with increasing sliding velocity. Regardless of the specific molecular mechanism, the decay of the stick−slip amplitude suggests that the pulled-out chains become progressively more aligned (shear-ordered or shear thinned) with time or sliding distance. It therefore takes less and less time to reach the critical shear stress as the number of stick−slip events increases; and after a certain number of stick−slips the alignment of the segments no longer changes, or their friction force no longer changes, whereupon the stick−slip disappears and merges into smooth sliding (so long as the surfaces continue to move at the same velocity).

The stop−start measurements support the above picture. These are equivalent to stopping the sliding, as on reversing, then continuing, but now in the *same* direction. After a short stop, the stiction spike is small, consistent with the interpenetration across the contact interface being small. The stiction spike increases as the stopping time is increased, consistent with a concomitant increase in interpenetration. It is interesting to speculate that the critical stopping or reversal time below which no stiction spike (or stick slip) will appear at the recommencement of sliding should correspond to the time taken for the last decaying stick−slip event before the system transits to smooth sliding.

Effect of Segment Polarity. UV radiation in the presence of oxygen gas leads to an increase of oxygen-containing hydrophilic groups at both of the polymer surfaces, as shown by contact angle measurements (Figure 19). Could this, then, be the cause of the dramatically increased adhesion and friction observed

for PS after UV radiation? The sol fraction data showed that UV radiation in the presence of oxygen results in cross-linking of the PVBC surfaces. Yet, the cross-linked but oxidized polar PVBC surfaces exhibited significantly *lower* friction and adhesion hysteresis than the untreated nonpolar PS or PVBC surfaces. We also compared the adhesion and friction of the PVBC surfaces that were cross-linked both in the presence and absence of oxygen and obtained very similar results. We further note that the adhesion hysteresis of untreated low MW PS surfaces is very high despite its being nonpolar. These results show that the polarity of the surfaces is not the main or even an important factor in determining the increased adhesion (hysteresis) and friction, and it may be further noted that "dipolar" interactions are generally much weaker than nonpolar (van der Waals−dispersion) interactions, except for very small molecules.[22]

Effect of Temperature. In another paper, we describe our results on lower MW PS surfaces as these pass through their glass transition temperature. As might be expected, instead of a continuing increase in the adhesion hysteresis and friction with decreasing MW, a point is reached where the polymer becomes more viscoelastic then fluid, which now lowers the adhesion and friction and totally changes the molecular mechanisms and deformations associated with these phenomena.

Correlating the Adhesion and Friction Forces and the Dynamics of the Surface Polymer Groups. Regarding the quantitative correlations between the measured adhesion hysteresis and friction forces, detailed theories, models, and computer simulations are highly complex. However, the following simple equation has been found to give good semiquantitative correlations between the adhesion hysteresis $\Delta\gamma$ and the adhesion energy contribution to the friction force F of two shearing surfaces[37]

$$F = \epsilon A \Delta\gamma/\delta \tag{4}$$

where A is the real contact area, $\Delta\gamma$ is defined by eq 3, and δ is the distance moved between collisions of the protruding or interpenetrating molecular groups (cf. Figure 20) or, more precisely, between the bonds that are continually broken and re-formed during sliding. The dimensionless parameter ϵ is the fraction of the kinetic energy transferred to the lattice per collision. It is therefore less than 1 and gives the fraction of the frictional energy that is commonly referred to as being "lost" or "dissipated" as frictional heat. In our SFA experiments three of the five parameters of eq 4, F, A, and $\Delta\gamma$, can be directly measured, and δ is estimated to be 1−2 nm from the above analysis. Previous fits of this equation to experimental data have found that ϵ lies between 0.2 and 1.0.[38]

Figure 21 shows a hysteretic JKR plot for UV treated (bond broken) PS 280 000 where $\Delta\gamma = 13.5$ mJ/m^2, and Figure 14 shows that the measured friction force at zero load for this system was $F = 5.8$ mN when the contact area was $A = 1260\ \mu$m^2. The parameter δ is taken to be 1.6 nm, corresponding to the previously estimated maximum penetration length of PS segments. Inserting these values into eq 4 we obtain $F = \epsilon A\Delta\gamma/\delta = 10.6\epsilon$ mN, which gives $\epsilon \approx 0.55$.

Unfortunately, we could not perform the same calculation for all the polymer surfaces studied. In the case of the cross-linked polymer the adhesion hysteresis $\Delta\gamma$ was too small to measure accurately, while for the chain-broken polymers the friction was too high to measure. The above example was chosen because the adhesion hysteresis, though low, was *large* enough to measure accurately, while the friction force was high, but sufficiently *low* to measure accurately. It also exemplifies, once again, that only a small adhesion hysteresis is needed to generate high friction forces.

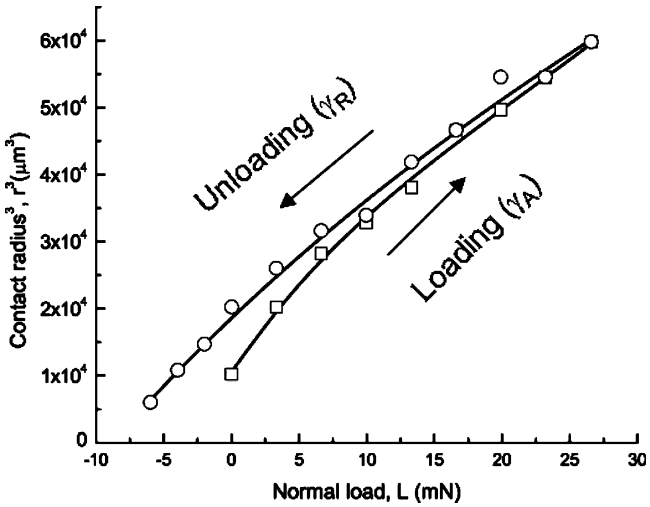

Figure 21. Hysteretic JKR loading and unloading plots for partially bond broken PS 280 000 after UV treatment for 480 min (8 h). The surface energy hysteresis, eq 1, was found to be $\Delta\gamma = (\gamma_R - \gamma_A) = 13.5\pm2.9$ mJ/m^2. Note the much longer radiation time of 14 h in Figure 5 resulting in unmeasurably high friction. The shorter time used here allowed a semiquantitative comparison between the adhesion hysteresis and friction forces. Errors are roughly the size of the data points.

Finally, as discussed in the text, the critical velocity V_c of ~1 μm/s suggests a relaxation time of $\tau_c \sim 1-2$ ms for the loops of untreated PS and PVBC to entangle/disentangle across the shearing interfaces *when confined under a finite adhesive contact pressure*. That this value is similar for these two polymers, and independent of MW in the range 100 000−2 000 000, is probably due to their very similar segmental structure and that the average surface loop size does not depend on the MW once it exceeds a certain value, e.g., the persistence length. Our results with the bond broken polymers, however, suggest that the relaxation time of free chain ends is much shorter. Our estimated relaxation time of 1−2 ms corresponds to an activation energy barrier of about 13 kcal/mol assuming a segmental correlation time of 500 fs.[26] This may be compared with a recent friction AFM study of a silicon tip sliding on a glassy PS surface by Sills and Overney[27] who found an activation energy barrier of 7 kcal/mol. We cannot say what molecular groups or relaxation modes are involved *at the surfaces, under compression, and during sliding*. The three literature values for the δ, β, and α relaxations of bulk PS are 2−3, 35, and 90 kcal/mol, respectively. This is consistent with our findings that the adhesion and friction are determined by local segmental motions (the δ and β modes) rather than the motions of whole molecules (α modes) which determine the glass transition.

Conclusions

We have studied the adhesion and friction forces between two glassy polystyrene and poly-vinylbenzyl chloride surfaces using a surface forces apparatus (SFA).

Cross-linking of the polymer surfaces reduce the adhesion and friction whereas increasing the number of the chain ends at the surfaces, either by scission or by addition of short chain polymers, leads to increased adhesion and friction. Only a small number of end segments are needed to produce large increases in the adhesion and friction forces but only if these segments are free to penetrate into the opposing surface.

Acknowledgment. We thank E. Kramer for helpful discussions and G. Carver for technical assistance. We thank E. B. Watkins, D. Doshi, and J. Majewski at Los Alamos Neutron Science Center for the neutron reflectometry measurements of the oxidized polymer surfaces. This work was supported by U.S. Department of Energy Grant DE-FG03-87ER 45331.

References and Notes

(1) Zisman, W. A. *Adv. Chem. Ser.* **1964**, *43*, 1.
(2) Kano, Y.; Akiyama, S. *J. Adhes. Sci. Technol.* **1992**, *6*, 1251−1264.
(3) Kano, Y.; Akiyama, S. *Polymer* **1992**, *33*, 1690−1695.
(4) Kilpadi, D. V.; Lemons, J. E. *J. Biomed. Mater. Res.* **1994**, *28*, 1419−1425.
(5) Johnson, K. L.; Kendall, K.; Roberts, A. D. *Proc. R. Soc. London Ser. A: Math. Phys. Sci.* **1971**, *324*, 301.
(6) Mangipudi, V. S.; Huang, E.; Tirrell, M.; Pocius, A. V. *Macromol. Symp.* **1996**, *102*, 131−143.
(7) Tirrell, M. *Langmuir* **1996**, *12*, 4548−4551.
(8) Sridhar, I.; Johnson, K. L.; Fleck, N. A. *J. Phys. D: Appl. Phys.* **1997**, *30*, 1710−1719.
(9) Luengo, G.; Pan, J. M.; Heuberger, M.; Israelachvili, J. N. *Langmuir* **1998**, *14*, 3873−3881.
(10) Hui, C. Y.; Lin, Y. Y.; Baney, J. M.; Jagota, A. *J. Adhes. Sci. Technol.* **2000**, *14*, 1297−1319.
(11) Li, L. H.; Tirrell, M.; Korba, G. A.; Pocius, A. V. *J. Adhes.* **2001**, *76*, 307−334.
(12) Maeda, N.; Chen, N. H.; Tirrell, M.; Israelachvili, J. N. *Science* **2002**, *297*, 379−382.
(13) Schmitt, F. J.; Yoshizawa, H.; Schmidt, A.; Duda, G.; Knoll, W.; Wegner, G.; Israelachvili, J. *Macromolecules* **1995**, *28*, 3401−3410.
(14) Chen, Y. L.; Helm, C. A.; Israelachvili, J. N. *J. Phys. Chem.* **1991**, *95*, 10736−10747.
(15) Yoshizawa, H.; Chen, Y. L.; Israelachvili, J. *J. Phys. Chem.* **1993**, *97*, 4128−4140.
(16) Yamada, S.; Israelachvili, J. *J. Phys. Chem. B* **1998**, *102*, 234−244.
(17) Ton-That, C.; Teare, D. O. H.; Bradley, R. H. *Chem. Mater.* **2000**, *12*, 2106−2111.
(18) Otocka, E. P.; Curran, S.; Porter, R. S. *J. Appl. Polym. Sci.* **1983**, *28*, 3227−3233.
(19) Onyiriuka, E. C. *J. Appl. Polym. Sci.* **1993**, *47*, 2187−2194.
(20) Israelachvili, J. N.; McGuiggan, P. M. *J. Mater. Res.* **1990**, *5*, 2223−2231.
(21) Luengo, G.; Schmitt, F. J.; Hill, R.; Israelachvili, J. *Macromolecules* **1997**, *30*, 2482−2494.
(22) Israelachvili, J. N. *Intermolecular & surface forces*, 2nd ed.; Academic Press: London, 1991.
(23) Fox, T. G.; Flory, P. J. *J. Polym. Sci.* **1954**, *14*, 315−319.
(24) Berman, A. D.; Ducker, W. A.; Israelachvili, J. N. *Langmuir* **1996**, *12*, 4559−4563.
(25) Gourdon, D.; Israelachvili, J. N. *Phys. Rev. E* **2003**, *68*.
(26) Adachi, K.; Saiz, E.; Riande, E. *Phys. Chem. Chem. Phys.* **2002**, *4*, 635−640.
(27) Sills, S.; Overney, R. M. *Phys. Rev. Lett.* **2003**, *91*, 095501.
(28) In the previous study[12] with high MW PS (240 000−2 000 000 Da) the number of chain ends were considered to be too low to allow one to detect effects arising from this difference and, indeed, no significant differences in the adhesion and friction forces were detected.
(29) We made errors in our previous report.[12] The average MW of the PVBC 25 000 Da was actually 100 000 Da, and the MW of the PS 100 000 Da was actually 280 000 Da.
(30) At any given L, one may define a critical velocity V_c above (or below) which stick−slip disappears. Likewise, at any given V, one may define a critical load L_c (or pressure) below or above which stick−slip disappears, as seen in Figure 10.
(31) When untreated surfaces are separated after prolonged contact the deformed edges slowly relax to the original flat shape. However, if the surfaces are cross-linked by UV radiation before the surfaces have regained their original shape, the deformed shape is preserved.
(32) It is more common to quantify adhesion hysteresis in terms of the difference between the receding and advancing surface energies ($\gamma_R - \gamma_A$). Often, however, the advancing energies are not very different (and close to the thermodynamic values), as was found to be the case here (see Figure 7), so that by far the greatest effect is the change in the receding energy γ_R.
(33) Three to five segments.
(34) In contrast to the advancing or "coming-on" adhesion energy, which is less variable and usually close to the thermodynamic equilibrium value.
(35) The relationship between the pull-off force and surface energy is surprisingly insensitive to the deformed shapes of the separating surfaces, being 25% different between highly deformable (but elastic) and totally rigid surfaces. This assumption may therefore be a reasonable one.
(36) In contrast to the "apparent" or macroscopic area.
(37) This equation applies to zero external load, L (Figure 1). In the presence of a compressive load the contact area in eq 4 increases, but there is also an additional purely load-dependent contribution.
(38) Strictly, the two measurements should be performed at the same velocity; i.e., the time taken for a loading-unloading cycle should equal the sliding time to traverse the distance δ.

MA047733E